

Supplementary figures

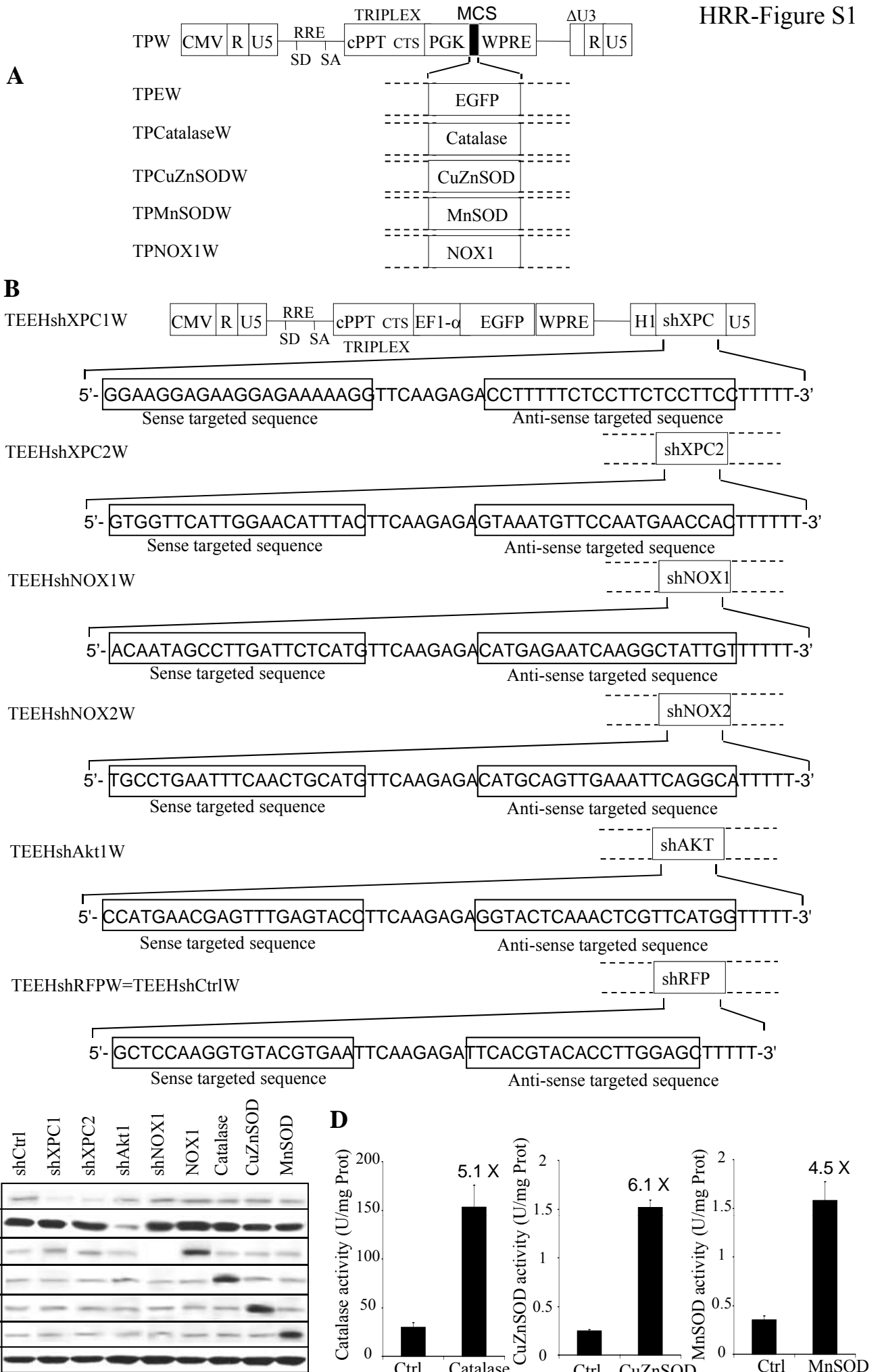


Figure S1. Vector constructs and analysis of the transduction efficiency. (A) Lentiviral vectors constructs used to overexpress EGFP, catalase, CuZnSOD, MnSOD, or NOX1 are shown. Vectors carry an internal cassette for the enhanced green fluorescent protein (EGFP), catalase, CuZnSOD, MnSOD, or NOX1 driven by the promoter of human phosphoglycerate kinase gene (hPGK). Δ U3, R, and U5 are the LTR regions, with a deletion that includes the enhancer and the promoter from U3. CMV is the cytomegalovirus promoter, SD is the major splice donor site, SA is the splice acceptor site, RRE is the rev-response element, cPPT is a nuclear import sequence, and WPRE is a regulatory element of woodchuck hepatitis virus. (B) Lentiviral constructs used to inhibit XPC, NOX1, NOX2, AKT, or red fluorescent protein (RFP) expressions are shown. TEEHshRFPW construct was used as the control shRNA (named shCtrl) plasmid. (C, D) Transduction efficacy was checked by western blotting analysis (C) and also by measuring the specific activity of each antioxidant enzyme in the keratinocytes (D) as described in the Methods section.

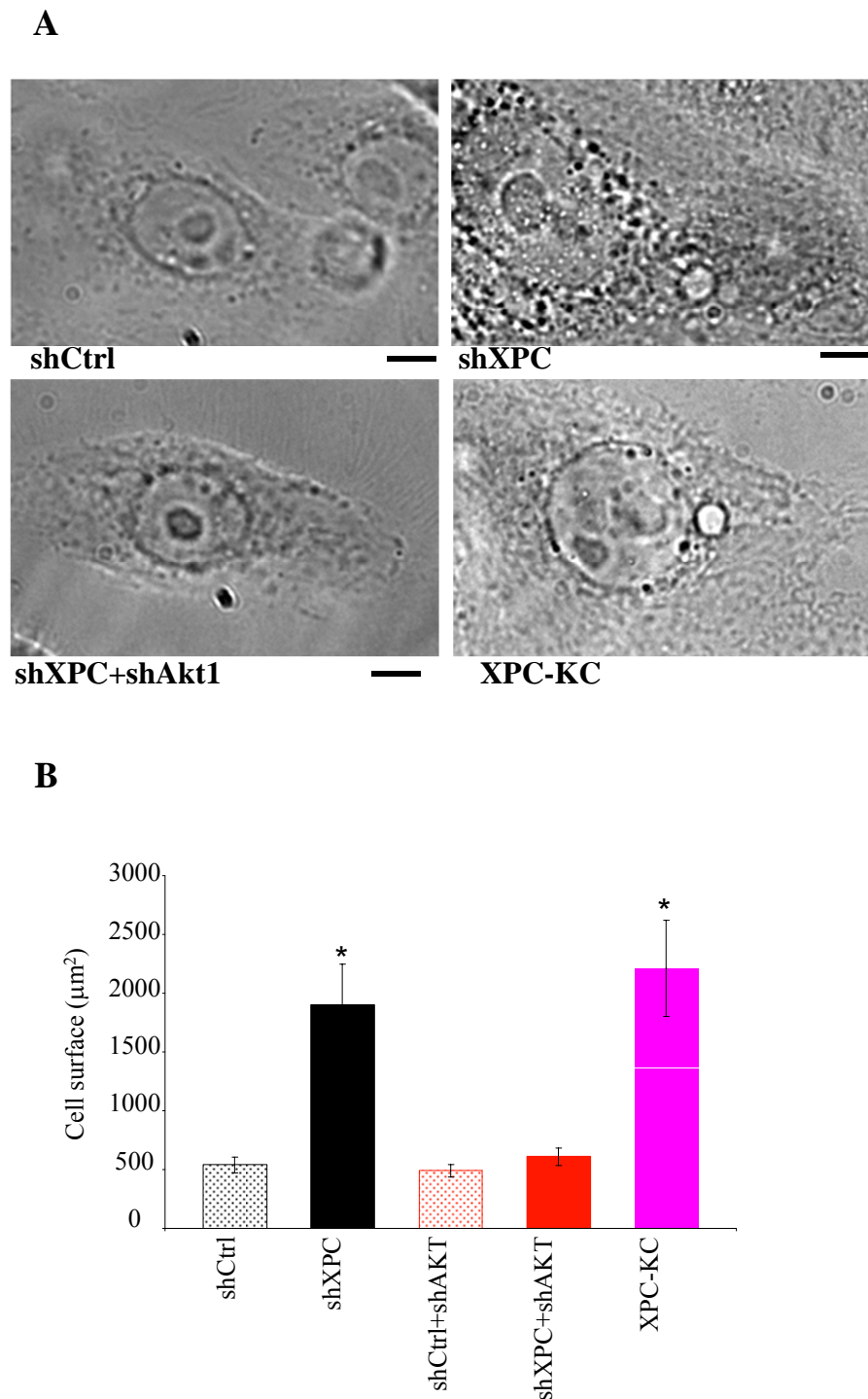


Figure S2. XPC downregulation results in change of keratinocyt cell size

At 15 days after transduction cells was photographed with light microscopy. **(A)** Light micrographs show that XPC^{KD^{NH}K} cells are larger than the control cells and that AKT downregulation inhibits this modification. **(B)** Surface of 100 cells (per condition) was measured. Results are expressed as average cell surface \pm SD of three independent experiments. *, $p < 0.05$ for different cells vs shCtrl-transduced cells.

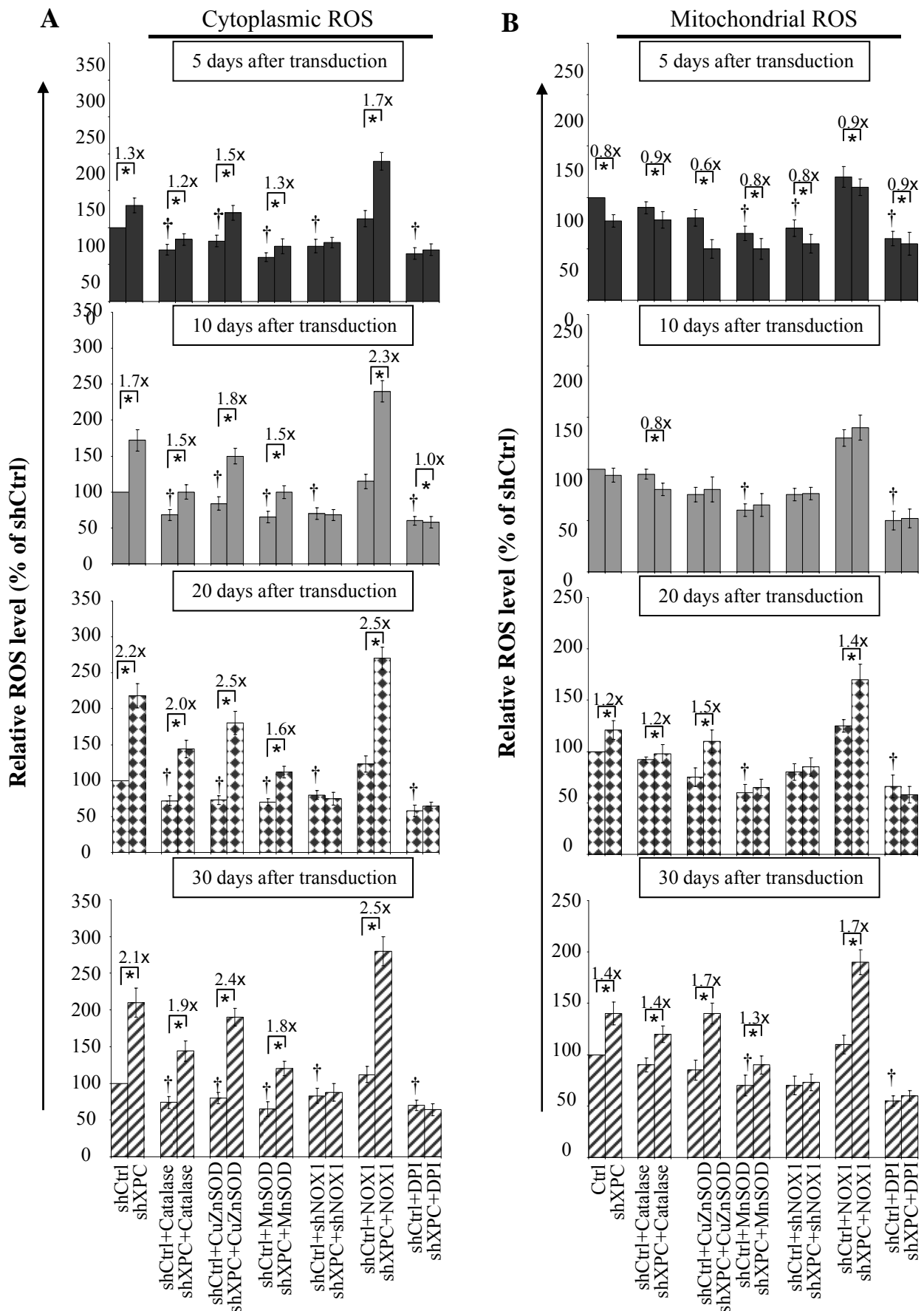


Figure S3. Inhibition of NOX1 expression blocks the effect of XPC downregulation on ROS levels. Intracellular ROS levels were measured in keratinocytes at different days following transduction using CM-H₂DCF-DA, the cytoplasmic probe, or MitoSOX, the mitochondrial probe. **(A, B)** Cytoplasmic **(A)** and mitochondrial **(B)** ROS levels were measured in keratinocytes transduced with shCtrl, shXPC, catalase, CuZnSOD, MnSOD, shNOX1, and/or NOX1, and DPI-treated cells by flow cytometry. Data are expressed as the mean \pm SD of three independent experiments. †, $p < 0.05$ for different cells vs shCtrl-transduced cells and *, $p < 0.05$ for different cells vs indicated corresponding samples.

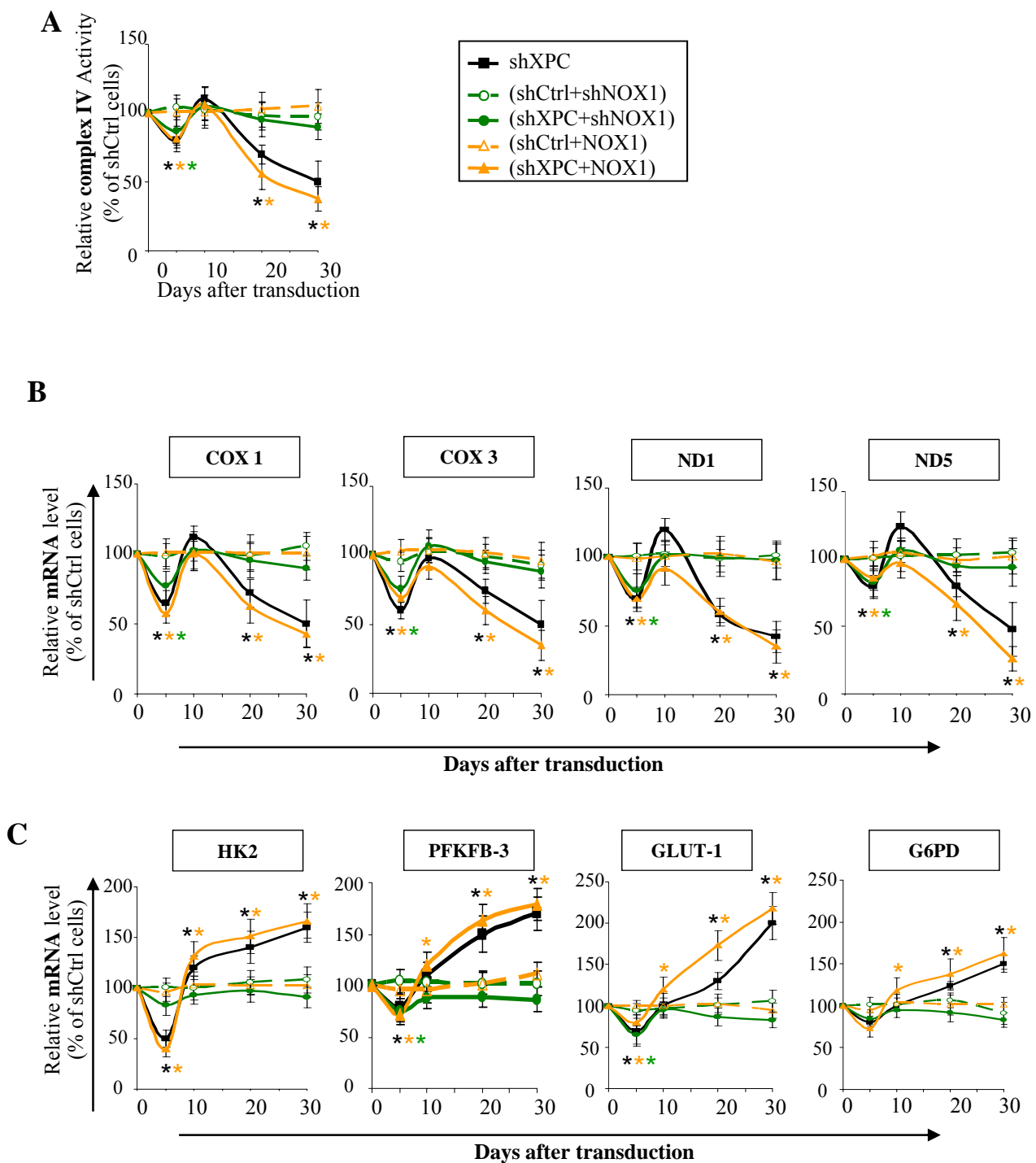
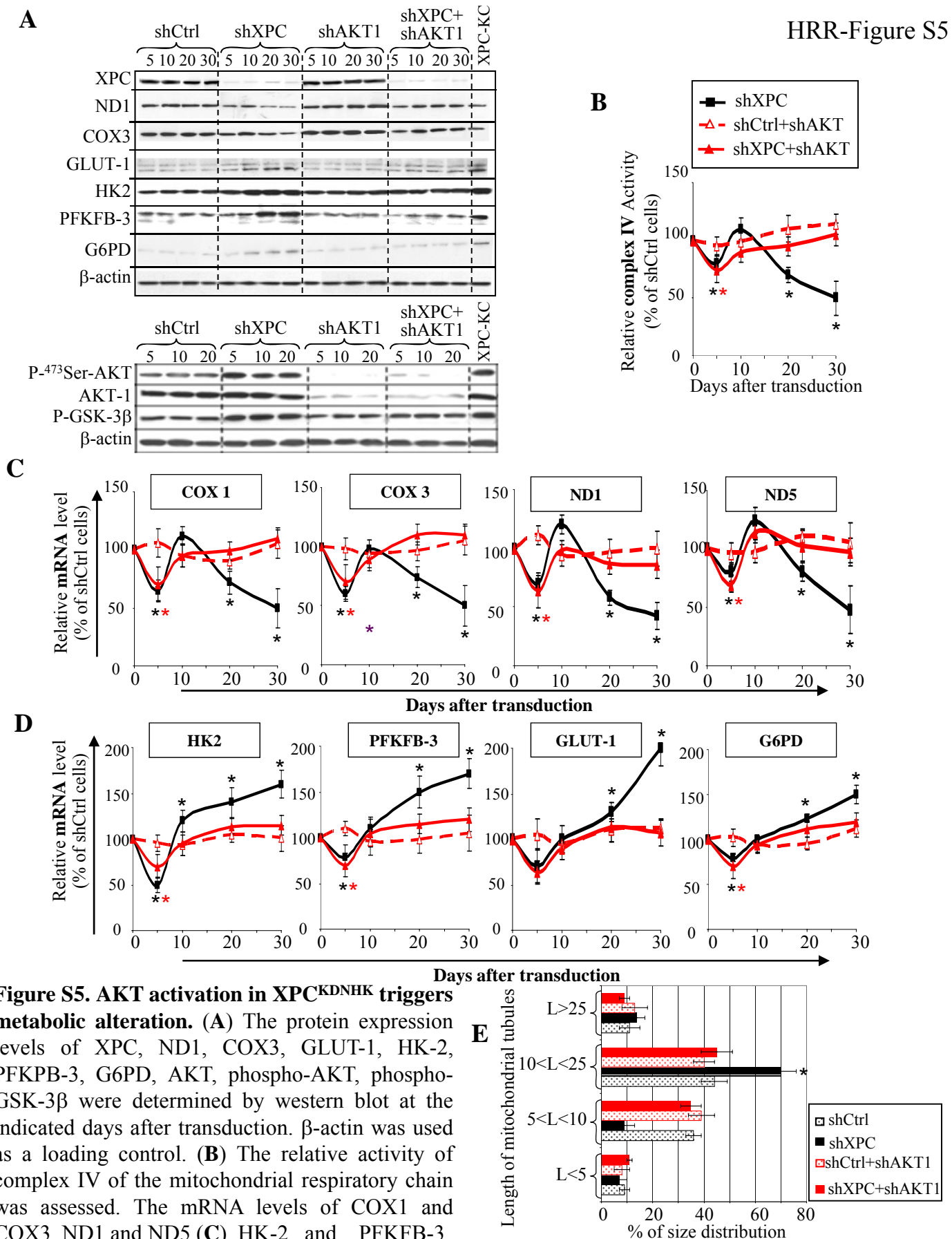


Figure S4. NOX1 activation in XPC^{KDNHK} triggers metabolic alteration. (A) The relative activity of complex IV of the mitochondrial respiratory chain was assessed. The mRNA levels of COX1 and COX3, ND1 and ND5 (B), HK-2 and PFKFB-3, and GLUT-1 and G6PD (C) were quantified by quantitative real-time RT-PCR at different time intervals following transduction. The results are shown as the average percentage of shCtrl \pm SD of six independent experiments. *, $p < 0.05$ for different cells vs shCtrl-transduced cells.



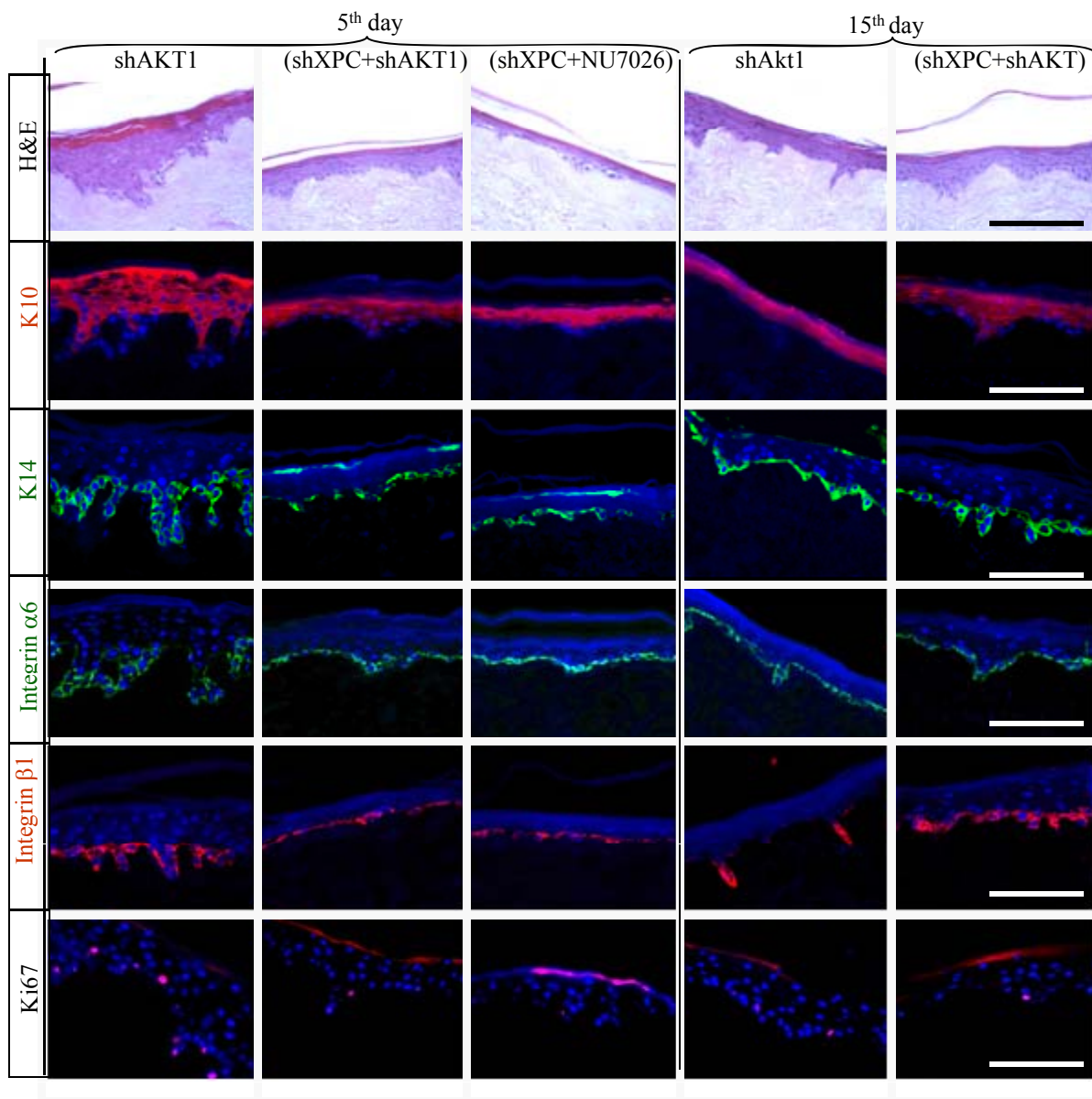


Figure S6. XPC silencing-induced epithelial hyperplasia manifestation blocked by AKT downregulation. Epidermis reconstructed with shAKT- and (shXPC+shAKT)-transduced keratinocytes on days 5 and 15 after transduction. The effect of DNA-PK inhibition on reconstruction of epidermis was assessed by treatment of epidermis with NU7026. Architecture of epidermis was evaluated with H&E staining. Proliferation and differentiation status of epidermis were assessed using immunofluorescence staining of K10, K14, integrin $\alpha 6$, integrin $\beta 1$, and Ki67. The nuclei were marked with DAPI and are in blue.

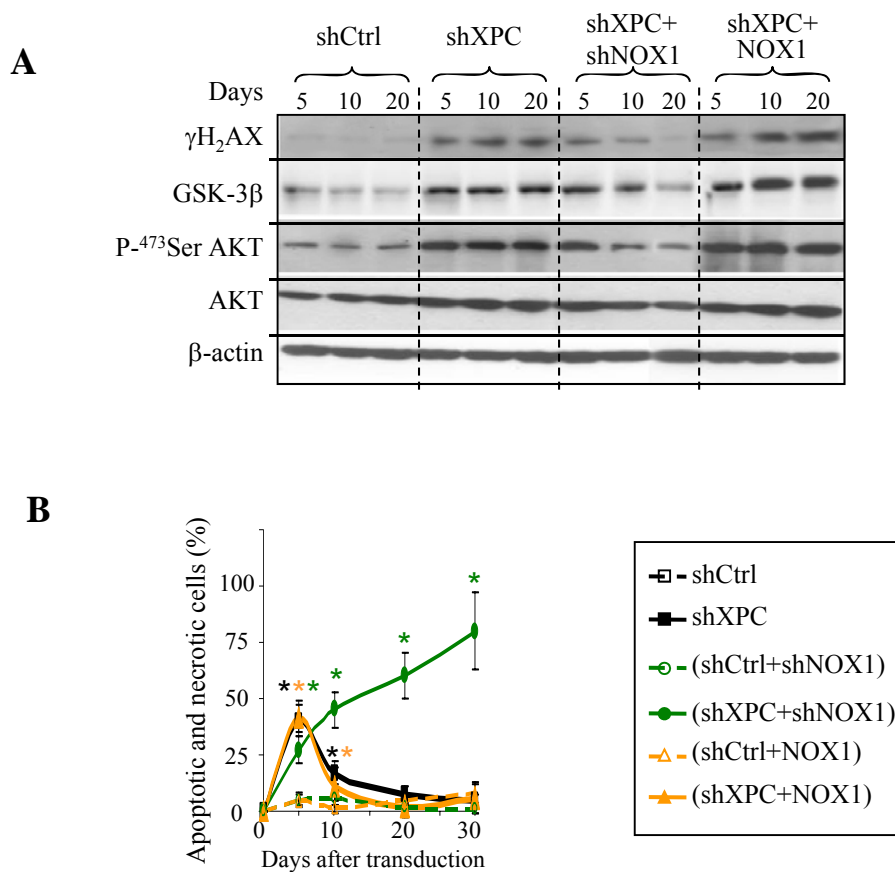


Figure S7. The effects of NOX1 on AKT activation in XPC^{KDNHK}. (A) The effects of NOX1 on the protein expression level of AKT, phospho-AKT, phospho-GSK-3 β and γ H₂AX were determined by western blot at the indicated days after transduction. β -actin was used as a loading control. (B) Apoptotic cells were analyzed by flow cytometry at indicated time intervals after transduction. Results are expressed as the average percentage of apoptotic and necrotic cells \pm SD of three independent experiments. *, $p < 0.05$ for different cells vs shCtrl-transduced cells at the indicated time points.

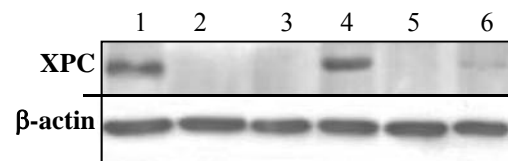


Figure S8. XPC protein level in cells from XPC patients. Total cell lysates from 3 patients (lanes 2, 3, and 5), 2 control samples (lanes 1 and 4), and one control sample transduced with shXPC (lanes 6) were analyzed by western blot and probed with anti-XPC and anti- β -actin antibodies. Anti- β -actin was used to normalize protein levels.

Supplementary Tables

Table S1. Primer sequences for quantitative real-time PCR

Target gene	SEQUENCE
ND1	F: ACGCCATAAAACTCTTCACCAAAG R: TAGTAGAAGAGCGATGGTGAGAGCTA
ND5	F: AGTTACAATCGGCATCAACCAA R: CCCGGAGCACATAAATAGTATGG
Cox I	F: CTGCTATAGTGGAGGCCGGA R: GGGTGGGAGTAGTTCCCTGC
Cox III	F: CCAATGATGGCGCGATG R: CTTTTTGGACAGGTGGTGTGTG
GLUT-1	F: GCTACAACACTGGAGTCATC R: GGATCAGCATCTCAAAGGAC
HK-1	F: GCTGGCCGATCAACACCGT R: GCCGTCCGGGGTAGCACA
PFKFB-3	F: GGTGTGCGACGACCCTAC R: GTACACGATGCGGCTCTG
G6PD	F: ATGATGCAGCCTCCTACCAG R: ACAGGGAGGAGATGTGGTTG
Ku70/XRCC6	F: CCGAGATACAGGCATCTTCC R: TCCGCAACAGGTCTTCTAGC
DNA-PKcs	F: CCTTGACACAGTTCCTGAGGT R: TCCTGAGAACTGGCCCTTTT
Tubulin	F: GAGTGCATCTCCATCCACGTT R: TAGAGCTCCCAGCAGGCATT

Table S2. Primer sequences used to detect mitochondrial deletions

Primer name	SEQUENCE	Position
A1*	5'-CTTTTGGCGGTATGCACTTT-3'	404-423
A2*	5'-GATTATGGATGCGGTTG TT-3'	4676-4657
B1*	5'-CAACCCTCGCCCATC CTA-3'	491-508
B2*	5'-CCTGCAAAGATGGTAGAGTAGATGAC-3'	4516-4489
C1 [†]	5'-GCAGTAATATTAATAATTTTCATG-3'	7293-7316
C2 [†]	5'-CTAGGGTAGAATCCGAGTATGTTG-3'	13298-13905
D1 [†]	5'-TGAACCTACGAGTACACCGA-3'	7091-7920
D2 [†]	5'-GGGGAAGCGAGGTTGACCTG-3'	13650-13631
Ref1*	5'-GATTTGGGTACCACCCAAGTATTG-3'	16042-16066
Ref2*	5'-AATATTCATGGTGGCTGGCAG TA-3'	16125-16102

* the primer sequences are according to Harbottle and Birch-Machin (Harbottle and Birch-Machin, 2006).

[†] the primer sequences are according to Berneburg *et al* (Berneburg et al., 1999).